Highly efficient anomalous reflection by ultrathin phase gradient planar meta-surface arrays in near infrared region

MIAN JIA[a], HUIHUI ZHU[b], DONGSHUO ZHU[c], WEIMIN WANG[a], GUOHUA SHI[d], XUFENG JING[a, *]
[a]*Institute of Optoelectronic Technology, China Jiliang University, Hangzhou 310018, China*
[b]*State Key Laboratory of Modern Optical Instrumentations, Department of Optical Engineering, Zhejiang University, Hangzhou 310027, China*
[c]*Institute of art and design, Renmin university of China*
[d]*Institute of Suzhou Biomedical Engineering, Chinese Academy of Sciences*

The higher efficient anomalous reflection performance in short wavelength region is carefully designed and numerically demonstrated based on an ultrathin phase gradient meta-surface arrays. These meta-surfaces, comprising a periodic arrangement of metal nanobricks configurations providing required phase shift for the reflected beam from 0° to 360°, exhibit a higher conversion efficiency of about 87% limited by Ohmic loss in the metal to anomalous reflection mode at normal incidence. Importantly, the light polarization of the anomalous reflection is same as that of the incident wave. The generalized Snell's law is verified by the near field propagating characteristics of a plane wave and the far field distribution. Compared with a conventional optical phase shifts components, new degrees of designed freedom can be attained by introducing this abrupt linear phase variation along the ultrathin planar interface. Based on these metasurfaces with the great flexibility in manipulation of light beam, some optical components with inaccessible functionalities by a traditional nanostructure can be realized. Further, the discrete elements in a unit array are replaced by the continuous one, in which the anomalous reflection phenomenon also arises.

(Received September 8, 2016; accepted April 6, 2017)

Keywords: Metasurface, Metamaterial, Anomalous reflection, Infrared region

1. Introduction

The discovery of metamaterial [1-3] was a significant breakthrough in materials science, since then there has been a sustained research interest in meta-material and a rush to discover its excellent physical properties. These "new substances" with extraordinary physical properties and unconventional electromagnetic properties which have not yet been found in nature can be obtained by precisely designing structures of material. Recently, a kind of two-dimensional metamaterials with ultrathin sub-wavelength thickness was proposed to be engineered for the planar optical devices, which is named as metasurfaces [4-8]. Based on flexible design and potentially application as modulator of the phase change of reflected/transmitted electromagnetic waves, metasurface has intrigued great research interests. The phase gradient of metasurface, governed by a generalized Snell's law, can be applied to provide greater flexibilities in molding propagations and wave-fronts of incident wave [9-10]. Interestingly, various structures of metasurfaces, including V-shaped antennas [11], Y-shaped antennas [11], H-shaped antennas [11], split-ring resonators [12], nanorods [12-13], and nanobricks [5], have been employed for beam steering or beam shaping, optical vortex plates, plasmonic lenses and polarization manipulation. However, most of researches on the meta-surface focus on its performance in the microwave regime, and relevant work is just extended to near-infrared (IR) regime [14]. Moreover, the anomalous reflected/refracted beams have different polarizations with the incident one, which is inconvenient for some application. And the upper bound to the efficiency of the devices is theoretically estimated to 25% [11].

In this paper, we focus on the design of the anomalous reflection of the gradient metasurface in shorter wavelength around 800nm, and it keeps light polarization unchanged after the anomalous reflection. The conversion efficiency to the anomalous reflection is as high as 87%. Also, the functionality of the polarization beam splitting can be revealed by different incident polarizations. The structure of our design is the metal-insulator-metal configurations, in which the top metal layer is periodic nanobricks array. This construction is easy achieved in experiment and solves the problem that the polarizations of anomalous reflected/refracted are not consistent with the incident ones.

2. Design and analysis

Typically, the metasurface which is different from the general interface can change the phase and polarization of light wave, resulting in that the propagation of light is no longer following the general form of reflection and refraction laws. Therefore, the generalized Snell's law should be applied to facilitate a further understanding of the mechanism of interaction between light and metasurface. An abrupt phase shift $\phi(r_s)$ is introduced on interface, which is the function of location, embodying phase change discontinuity. Assuming that the phase gradient $d\phi/dx$ along the interface is a constant, the generalized Snell's law is described for reflection as [9]

$$\sin(\theta_r) - \sin(\theta_i) = \frac{\lambda_0}{2\pi n_i}\frac{d\Phi}{dx} \quad (1)$$

where θ_r and θ_i are the angle of reflection and incident, respectively; dx is the distance between the crossing points; $d\Phi$ is the phase variation between the crossing points; n_i is the refractive indice of the media on the incident side; and λ_0 is the vacuum wavelength. Based on Eq.(1), it is found that as long as an appropriate phase gradient along the interface ($d\Phi/dx$) is introduced, the reflected beam can have an arbitrary direction. Therefore, it is crucial to design certain structure to achieve phase gradient. In our study, the finite difference time domain (FDTD) method is applied to accurately analysis reflection efficiency and field distribution of the meta-surface [15].

The designed structure of the nanobricks is schematically shown in Fig. 1, with a unit cell presented in the inset. In the inset of Fig. 1, the structure is divided into three layers: the bottom layer is thick gold substrate overlaid by a thin SiO_2 layer (the refractive index of 1.45) and the top layer is a gold nanobrick. The depths of the top layer, SiO_2 layer and the gold substrate are denoted by d_1, d_2 and d_3, respectively. The length and width of the top layer, respectively, are represented by L_x and L_y. The meta-surface works in the short wavelength of 800 nm. In our design, the depths of layers are d_1=50 nm d_2=50 nm, and d_3=130 nm, respectively. In order to realize high reflection, the unit cell of metasurface was designed with the thick d_3 and the thin d_1 and d_2. For this sandwich structure, the Au nanobricks and the Au substrate are nearby, the strong near-field coupling can induce a magnetic resonance at a particular frequency [8]. Obviously, geometrical parameters of the structure are crucial to the magnetic resonance, so the size of the nanobricks is most important to the phase of the reflected light. So, the reflection phase delay of each structural unit can be efficiently designed by changing the L_x and L_y. Fig. 2 presents the reflective amplitude and phase with the direction of the incident electric field along x as a function of L_x and L_y. Then, in view of the criterion that the reflective amplitudes should be higher, and the reflective phase delays maintain about $\pi/4$ for each unit cells, the eight different sizes of nanobrick were chosen (Fig. 3a). It can be seen in Fig. 3(b) that the reflective phase covers near 360°, and its interval is about 45° for the eight nanobricks structures. It is apparent that the reflective amplitudes vary a little and the average value is over 0.90.

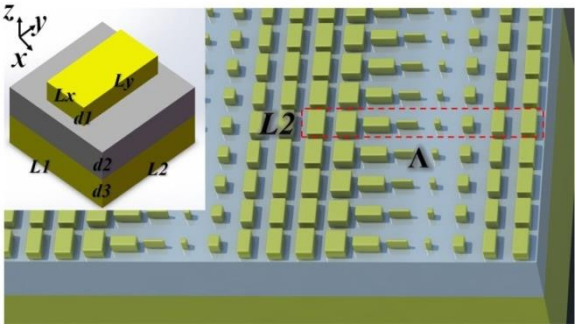

Fig. 1. Schematic diagram of our meta-surface with a unit cell (inset) consisting of a Au nanorod (yellow) and a continuous Au film (yellow) separated by the thin SiO_2 layer. A super cell of the sample (region surrounded by dashed line) consists of 8 unit structures with lengths (Lx) of top Au nanorods as 140,160,210,170,50,90,100 and 120 nm and widths (Ly) of top Au nanorods as 200,170,80,20,40,90,180 and 200nm. Other parameters are fixed as Λ=1920 nm, L1 = 240 nm, L2 = 240 nm, d1 = 50 nm, d2 = 50 nm and d3 = 130 nm

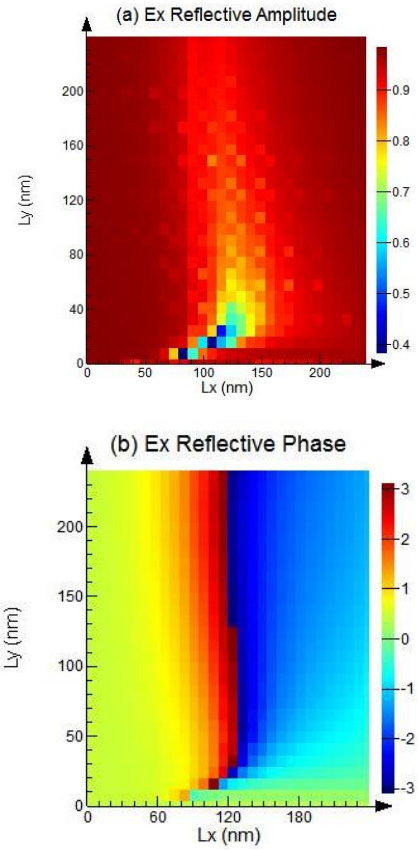

Fig. 2. (a) Reflective amplitude with the variation of the size and aspect ratio of the nanobricks. (b) Reflective phase with the variation of the size and aspect ratio of the nanobricks

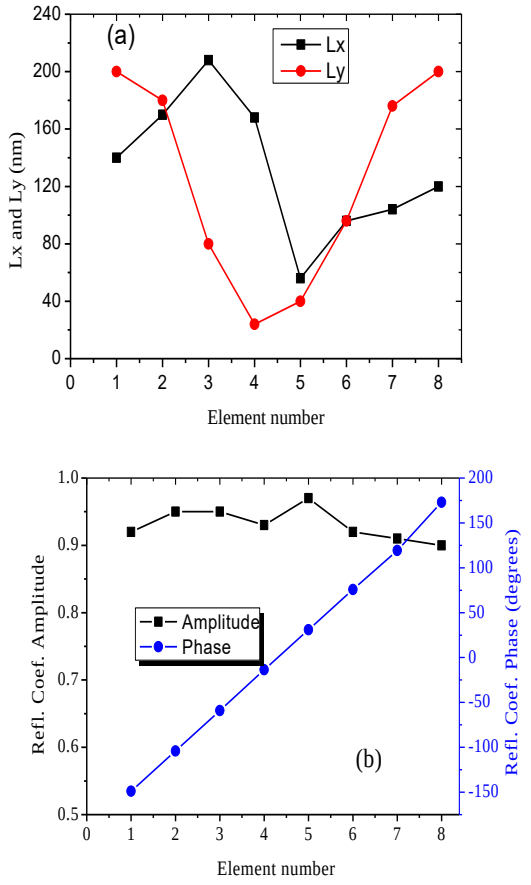

Fig. 3. (a) Lateral dimensions of eight different nanobricks designed to produce equidistant (within 2π range) phase shifts. (b) The reflection amplitudes and phases of eight nanobricks

In Fig. 4, the reflective electric field distribution is depicted. It indicates that the plane wave at normal incidence is titled by 22° as it passed through the eight nanabricks arrays metasurface. In other words, the plane wave with E_x polarization appears anomalous reflection. From Eq.(1), the phase delays Φ is 45° for each unit cell, so it can be assumed that the gradient of Φ is a constant, which means $\partial\Phi/\partial x=\xi$. It is clear to show that $\xi = 2\pi/L_x \approx 0.38\ k_0$ where L_x=1920 *nm* is the length of the period configuration and $k_0 = 2\pi/\lambda$ is the wavevector at λ = 800 *nm*. When the plane wave is normally incidence, i.e. $\theta_i = 0^o$, the reflect wave will propagate along an angle $\theta_r = \sin^{-1}(0.38) \approx 22.4^o$ according to the generalized Snell's law [16-18], which is in agreement with the simulation result.

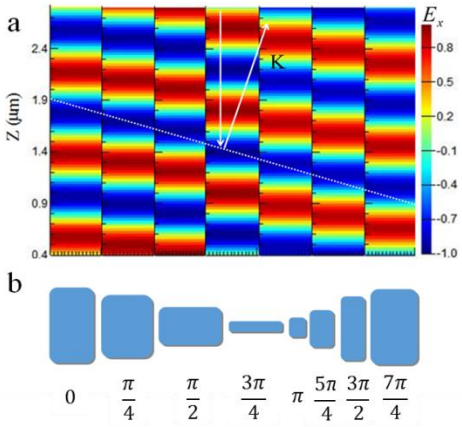

Fig. 4. FDTD simulated reflective E_x field distribution with the illumination of a normally E_x polarization plane wave on the eight nanobricks arrays. The dashed line is defined as the wavefront

In order to further quantitatively verify the generalized Snell's law and visualize these highly anomalous reflection behaviors, we numerically simulated the patterns of reflective field distribution with four representative incident angles of -10^o, 0^o, 10^o, and 40^o. The results are indicated in Fig. 5(a)-(d), respectively. It can be seen that the reflect angle is 22° when it is normally incidence. In the case of the incident angle attaining -10° in Fig. 5(b), it shows clearly that the incident beam is "negatively" reflected at the angle of 12° by our designed metasurface. Although the "positive" reflective angle of 32° is demonstrated in Fig. 5(c) for the incident angle of 10°, the reflective beam is nonspecular. Interestingly, the reflective wave is a well-defined surface wave bounded at the metasurface when the incident angle achieving to 40° as shown in Fig. 5(d). Based on the generalized Snell's law at the oblique incidence case [4], the reflection angle θ_r is derived as $\theta_r = \sin^{-1}(\sin\theta_i + \xi/k_0)$. Taking the case that incident angle is 10° as an example, the theoretical reflection angle is $\theta_r = \sin^{-1}(\sin 10^o + 0.38) = 33.6^o$. So the FDTD simulations results perfectly match with the theoretical value of the generalized Snell's law. Moreover, one should consider a critical angle $\theta_{ic} = \sin^{-1}(\sin 90^o - \xi/k_0)$, when $\theta_i > \theta_{ic}$, then the reflected beam becomes a surface waves that propagates along the interface. To our designed structure, the $\theta_{ic} = 38^o < 40^o$, so it is easy to explain the weak anomalous reflection when the incident angle is 40°. The characteristics of the anomalous reflection for our designed metasurface can be also revealed intuitively by the far field distribution as shown in Fig. 6. As depicted in Fig. 7, the meta-surface supports normal reflected beams with E_y polarized incident wave. Thus, our designed metasurface can be applied as a polarization beam splitter.

The reflectivity performance to our designed metasurface is indicated in Fig. 8 as a function of the incident angle of -10^o, 0^o, 10^o, and 40^o, respectively. It

can be seen that the anomalous reflectivity can reach to 87% at the designed wavelength of 800nm at the normal incidence in Fig. 8(a). Also, with the increase of the incident angle, the reflectivity is increased as shown in Fig. 8(b)-(d). So the designed gradient metasurface shows a broadband high efficient anomalous reflection, with the reflectivity being limited to about 94% because of Ohmic losses in the metal.

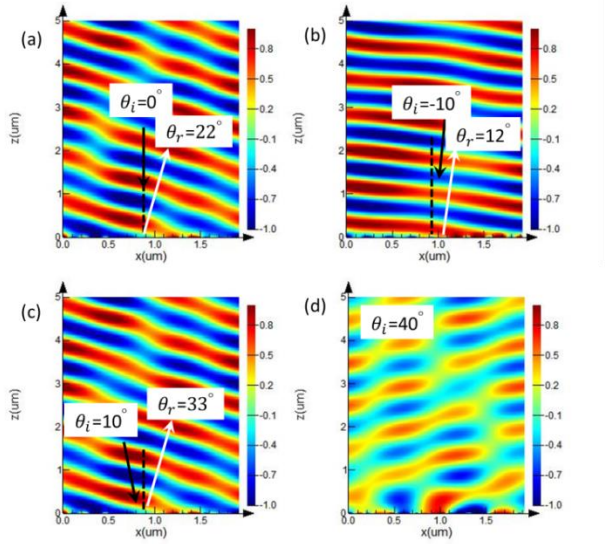

Fig. 5. Near field distributions of the reflective E_x when the incident wave of E_x polarization with the incident angle of (a) 0°, (b) -10° , (c) 10°, and (d) 40°

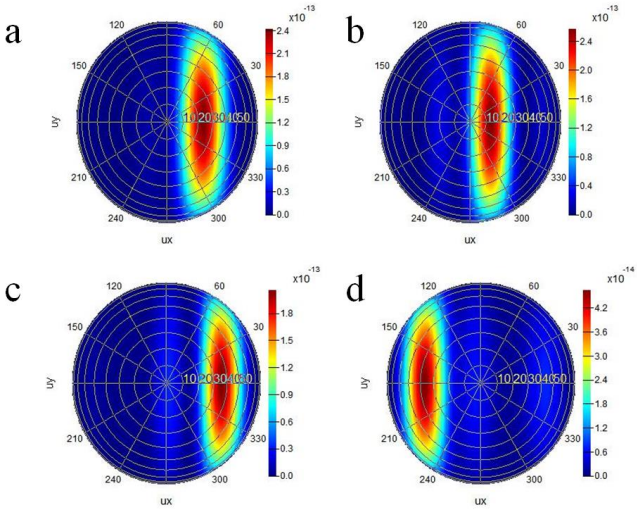

Fig. 6. Far field distributions of E_x when the incident wave of E_x polarization with the incident angle of 0°, (b) -10°, (c)10°, and (d) 40°.

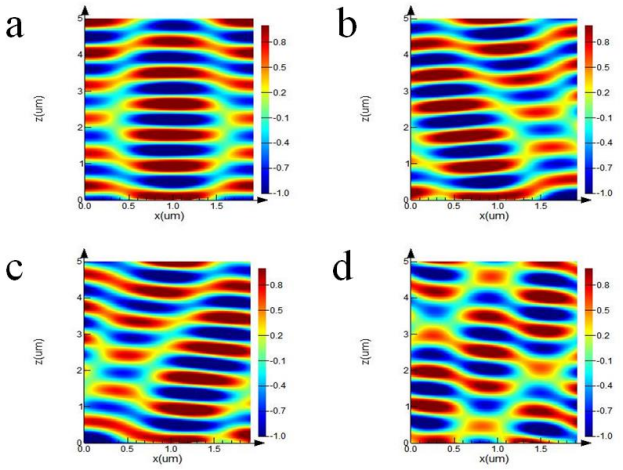

Fig. 7. Near field distributions of the reflective E_y when the incident wave of E_y polarization with the incident angle of (a) 0°, (b) -10° , (c) 10°, and (d) 40°

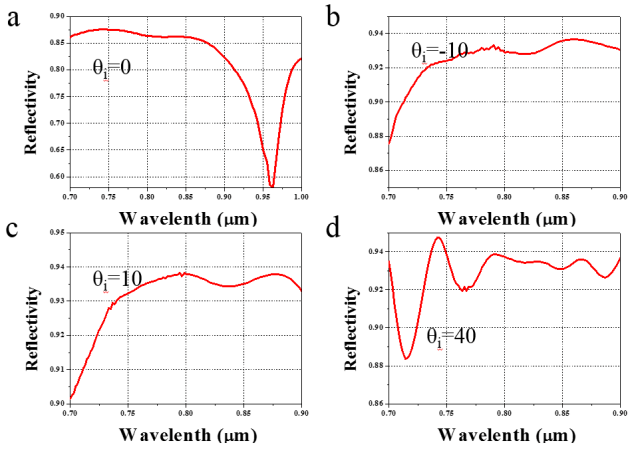

Fig. 8. The high efficient reflectivity performance when the incident wave of E_x polarization with the incident angle of 0°, (b) -10°, (c)10°, and (d) 40°

In addition, a unit cell depicted in Fig. 4.b can be reconstituted as a continuous structure, depicted in Fig. 9. The polynomial is used to fit the continuous profile and build the outline of continuous structure. It intrigues our interests about the reflected phenomenon when the plane wave through the continuous structure. It is surprising that the anormal reflection effect is still emerged as the configuration changed to continuous ones. From the far field distributions in Fig. 10, the propagated direction of reflected wave appears deviations when the incident angles are 0° and -10°. It worth mention that continuous metasurface can keep the phase adjustment continuity compared to discrete metasurfaces. However, compared to discrete strucutre, the phase interruption disappeared on the continuous ones. According to equation (1), the phase interruption would appear on the gap between two unit cells when the metasurface is discretized.

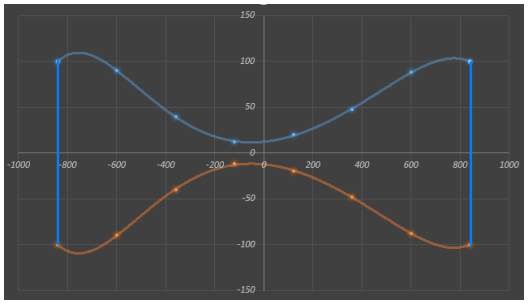

Fig. 9. Schematic diagram of continuous metasurface structure. The specific expressions are:

$$y_1 = -2\times10^{-16}x^6 + 10^{-13}x^5 - 3\times10^{-11}x^4 - 10^{-7}x^3 + 0.0003x^2 + 0.0268x + 12.384$$

$$y_2 = 2\times10^{-16}x^6 - 10^{-13}x^5 + 3\times10^{-11}x^4 + 10^{-7}x^3 - 0.0003x^2 - 0.0268x - 12.384$$

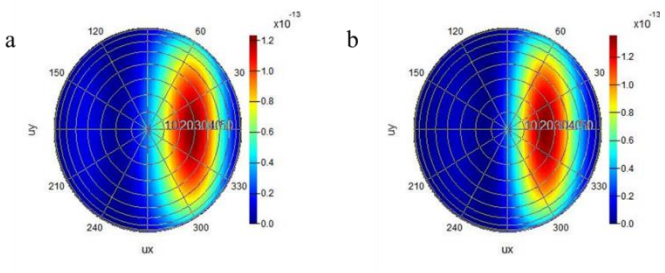

Fig. 10. Far field distributions of E_x when the incident wave of E_x polarization with the incident angle of (a) 0°, (b) -10°

3. Conclusions

In conclusion, we designed a phase gradient metasurface at the shorter wavelength of 800 nm with the high efficient anomalous broadband reflection. The generalized Snell's law is verified by theoretical derivations and numerically simulations. Compared to previously studied metasurfaces in the long wavelength regime, our metasurface with nanobricks configurations works in a shorter wavelength, and the anomalous reflected wave has higher conversion efficiency with the same polarization as incident wave. Furthermore, inspired by the discrete structure, a type of continuous metasurface is proposed, which offers a continuously varying phase and anormal reflection. Our designed results can results in many practical applications, such as polarization spectral beam splitters and wave plates. Especially, the continuous metasurface can pave a new approach to design flat optical components.

Acknowledgment

The authors acknowledge the support from Natural Science Foundation of Zhejiang Province (LY17F050009), National Natural Science Foundation of China (NSFC) (No. 61405182, No. 61675226, and No. 51401197), the National Instrumentation Program(2016YFF0102000),the Jiangsu Province Science Fund for Distinguished Young Scholars (BK20060010), the Frontier Science research project of the Chinese Academy of Sciences (QYZDB-SSW-JSC03), the Strategic Priority Research Program of the Chinese Academy of Sciences (XDB02060000) and Zhejiang Students Research and Innovation Team Funded Projects (2016R409009).

References

[1] Z. Yang, F. Gao, Y. Hou, D. Hu, L. Pang, X. Wu, Chin. Opt. Lett. **14**, 061602 (2016).
[2] T. Bu, K. Chen, H. Liu, J. Liu, Z. Hong, S. Zhuang, Photon. Res. **4**,122 (2016).
[3] Z. Li, C. Luo, G. Yao, J. Yue, J. Ji, J. Yao, F. Ling, Chin. Opt. Lett. **14**, 102303 (2016).
[4] A. Pors, M. Nielse, R. Erikse, Nano Lett. **13**(2), 829 (2013).
[5] S. Sun, K. Yang, C. Wang, Nano Lett. **12**(12), 6223 (2012).
[6] Q. Sun, S. Wang, H. Liu, S. Zhu, Chin. Opt. Lett. **14**, 051101 (2016).
[7] N. Yu, F. Aieta, P. Genevet, Nano Lett. **12**(12), 6328 (2012).
[8] L. Xin, X. Shiyi, C. Bengeng, Opt. Lett. **37**(23), 4940 (2012).
[9] N. Yu, G. Patrice, A. Kats, Science **334**, 333 (2011).
[10] X. Tian, Z. Li, Photon. Res. **4**(4), 146 (2016).
[11] N. Yu, C. Federico, Nat. Mater. **13**(2), 139 (2014).
[12] J. Zhou, T. Koschny, M. Kafesaki, Phys. Rev. Lett. **95**(22), 223902 (2005).
[13] C. Yan, Z. Su, E. Gu, T. Cao, J. Yang, J. Liu, Rsc. Advances **2**(28), 10481 (2012).
[14] X. Ni, N. K. Emani, A. V. Kildishev, A. Boltasseva, V. M. Shalaev, Science **335**, 427 (2012).
[15] S. Castillo, S. Omick, J. Electromagnetic Wave **8**(9), 1193 (2012).
[16] X. Zhao, J. Zhang, K. Fan, G. Duan, G. Metcalfe, M. Wraback, X. Zhang, R. Averitt, Photon. Res. **4**(3), A16 (2016).
[17] F. Aieta, P. Genevet, N. Yu, M. A. Kats, Z. Gaburro, F. Capasso, Nano Lett. **12**(3), 1702 (2012).
[18] X. Ni, A. V. Kildishev, V. M. Shalaev, Nat. Commun. **4**(4), 657 (2013).

*Corresponding author: jingxufeng@cjlu.edu.cn